Journal of Hazardous Materials 186 (2011) 1462–1473

Contents lists available at ScienceDirect

Journal of Hazardous Materials

journal homepage: www.elsevier.com/locate/jhazmat

Optimizing adsorption of crystal violet dye from water by magnetic nanocomposite using response surface modeling approach

Kunwar P. Singh[a,*], Shikha Gupta[a], Arun K. Singh[a], Sarita Sinha[b]

[a] Environmental Chemistry Division, Indian Institute of Toxicology Research, (Council of Scientific & Industrial Research), Post Box 80, Mahatma Gandhi Marg, Lucknow 226 001, India
[b] National Botanical Research Institute, (Council of Scientific & Industrial Research), Rana Pratap Marg, Lucknow 226 001, India

ARTICLE INFO

Article history:
Received 13 July 2010
Received in revised form
27 September 2010
Accepted 7 December 2010
Available online 14 December 2010

Keywords:
Magnetic nanocomposite
Crystal violet dye
Adsorption, Central composite design
Optimization
Response surface modeling

ABSTRACT

A magnetic nanocomposite was developed and characterized. Adsorption of crystal violet (CV) dye from water was studied using the nanocomposite. A four-factor central composite design (CCD) combined with response surface modeling (RSM) was employed for maximizing CV removal from aqueous solution by the nanocomposite based on 30 different experimental data obtained in a batch study. Four independent variables, viz. temperature (10–50 °C), pH of solution (2–10), dye concentration (240–400 mg/l), and adsorbent dose (1–5 g/l) were transformed to coded values and a second-order quadratic model was built to predict the responses. The significance of independent variables and their interactions were tested by the analysis of variance (ANOVA) and *t*-test statistics. Adequacy of the model was tested by the correlation between experimental and predicted values of the response and enumeration of prediction errors. Optimization of the process variables for maximum adsorption of CV by nanocomposite was performed using the quadratic model. The Langmuir adsorption capacity of the adsorbent was determined as 81.70 mg/g. The model predicted maximum adsorption of 113.31 mg/g under the optimum conditions of variables (concentration 240 mg/l; temperature 50 °C; pH 8.50; dose 1 g/l), which was very close to the experimental value (111.80 mg/g) determined in batch experiment.

1. Introduction

Crystal violet (CV), a synthetic basic cationic dye imparts violet color in aqueous solution. The cationic dyes are more toxic than the anionic dyes [1], as these can easily interact with negatively charged cells membrane surfaces, and can enter into cells and concentrate in cytoplasm [2]. CV is a typical triphenylmethane dye, which is widely used in textile dyeing industries, as a biological stain, dermatological agent, veterinary medicine, additive to poultry feed to inhibit propagation of harmful bacteria [3]. CV is toxic to mammalian cells and also a mutagen, mitotic poison [4] and a proven potent carcinogen [5]. It is responsible for moderate eye irritation, causing painful sensitization to light. It can cause permanent injury to the cornea and conjunctiva [6]. Inhalation of CV may cause irritation to the respiratory tracks, vomiting, diarrhea, pain, headache, and dizziness. Long term exposure may cause damage to the mucous membrane and gastrointestinal tract [7].

The color in water bodies reduces penetration of sunlight to the lower layers and hence, affects the aquatic life. Water soluble dyes are characterized by their poor biodegradability and it is estimated that about 20% of the total dye remains in the effluent during the production process [8]. With the legislations becoming more stringent, considerable importance has been given to the treatment of the dye containing effluents. Therefore, it is highly desirable to remove the dyes in general and CV in particular from water/wastewater.

Since, the synthetic dyes are inherently prepared as stable and non-degradable molecules, the conventional treatment methods are not suitable for their removal from aqueous phase [8]. However, over the years, the possibility of techniques such as oxidative degradation [9], electro-coagulation [10], membrane based separation process [11], and biochemical degradation [12] have been exploited, but these methods possess drawbacks due to their inapplicability to large scale units along with both energy and chemical intensiveness. Nevertheless, adsorption is shown to be potentially powerful method for dye removal from aqueous phase because of its easy operation, inexpensive, insensitivity to toxic substances, ability to treat concentrated forms of the dyes, and the possibility of re-using the spent adsorbent via regeneration [13]. Subsequently, a variety of activated carbon based adsorbents derived from various materials have been investigated for their efficacy and efficiency for the removal of dyes [14]. However, the large volume of the wastewater with high dye concentration has been compelling for

* Corresponding author. Tel.: +91 522 2476091; fax: +91 522 2628227.
E-mail addresses: kpsingh_52@yahoo.com, kunwarpsingh@gmail.com (K.P. Singh).

0304-3894/$ – see front matter © 2010 Elsevier B.V. All rights reserved.
doi:10.1016/j.jhazmat.2010.12.032

development of some non-toxic low cost efficient adsorbent with the possibility of regeneration for reuse. Unfortunately, activated carbons are difficult to separate from the solution and have been discarded with the process sludge after use in water and wastewater treatment, resulting in secondary pollution [15]. The magnetic adsorbents allow their separation from liquid phase by simply applying a magnetic field [16]. Magnetized materials have recently been employed for the water purification due to easy control and fast separation [17,18]. The magnetized adsorbents have recently been used for removal of dyes and other molecules from water [19–21]. The higher adsorption capacity of the magnetic adsorbents for basic cationic dyes has been attributed to the interactions of the hydroxyl groups with the dyes molecules [22].

In adsorption based methods, it is desirable to have knowledge of the process variables and their influence on adsorption capacity in order to maximize the contaminants removal efficiency of the adsorbents. The liquid–solid interface adsorption process is mainly influenced by the initial concentration of the adsorbate, initial pH of the solution, adsorbent dose, surface area of the adsorbent, contact time, operating temperature and the agitation speed. Optimization of the process variables is required to achieve the maximum adsorption capacity, and hence, the removal efficiency of the adsorbent. The conventional approach for optimization of process variables requires a very large number of experiments to be performed, which would be very expensive and time consuming. Moreover, it does not reveal the influence of the interactions between the process variables on the dependent variable [23]. Recently, Singh et al. [24] reported the linear (partial least squares) and non-linear (artificial neural networks) modeling approaches to predict the adsorption capacity of carbon for removal of phenol from aqueous solution. However, it required a large number of batch experiments to be performed. Such a limitation may be overcome by the statistical experimental design approach, which reduces the number of experiments as well as provides appropriate model for process optimization, allowing for the evaluation of the influence of inter-variable interactions on the process outcome. Recently, several types of experimental design methods have been employed in multivariable chemical process optimization [25]. Response surface modeling (RSM) is a useful method for studying the effect of several variables influencing the responses by varying them simultaneously and carrying out a limited number of experiments. A very limited number of studies employing the experimental design and optimization modeling approach for adsorption process have been reported in literature [23,25–27]. However, there is no information available in literature regarding the optimization of CV dye adsorption on magnetic nano-composites.

In view of the above facts, the specific objectives of the present study were: (1) to apply a four-factor central composite experimental design combined with RSM and optimization modeling for maximizing the adsorption capacity of the developed magnetic nanocomposite for CV dye removal from aqueous solution; (2) to examine the effects of four independent variables (initial concentration of dye, initial pH of solution, adsorbent dose, and operating temperature) and their interactions on the adsorption capacity of the nanocomposite for CV dye; and (3) to verify the validity of the proposed model by additional batch experiments conducted in the experimental range of the CCD..

2. Materials and methods

2.1. Response surface modeling

Response surface modeling (RSM) is an empirical statistical technique that uses quantitative data obtained from appropriately designed experiments to determine regression model and operating conditions [25–28]. The main objective of RSM is to determine the optimum set of operational variables of the process [29]. The statistical experimental designing of an adsorption process can reduce the process variability, experimentation time, overall cost with improved process output [30]. The RSM approach has widely been applied in chemical engineering and sorption process optimization [26].

Central composite design (CCD) has widely been used for fitting a second-order model and it requires a minimum number of experiments to be performed. For a 2 level study, the total number of experiments to be performed in this type of design are generally given as sum of the 2^n factorial runs, $2n$ axial runs, and n_c center runs ($2^n + 2n + n_c$), where n is the number of independent process variables. In CCD, the factorial or fractional factorial (2^n) levels are coded as ± 1, augmented by the $2n$ axial points $(\pm\alpha, 0, 0, \ldots, 0)$, $(0, \pm\alpha, 0, \ldots.., 0), \ldots.., (0, 0, \ldots.., \pm\alpha)$, and n_c, the center points $(0, 0, 0, \ldots.., 0)$. The number of center points (replicates) depends on the number of variables considered in the design and is generally between 3 and 10 [29]. The value of α is computed as 1/4th power to the number of factorial runs. Here, for the four variables studied at two levels, $\alpha = (2^4)^{1/4}$. In CCD, main effects and interactions between the variables may be estimated by performing a minimum number of experiments.

The optimization involves estimation of the coefficients in a mathematical model and predicting the response and checking the adequacy of the model. The response model may be expressed as [23];

$$Y = f(X_1, X_2, X_3, \ldots., X_n) \pm e \quad (1)$$

where, Y is the response, f is the response function, X_i are the independent variables, and e is the experimental error. The form of response function, f is unknown and may be very complicated. It largely depends on the nature of relationship between the response and the independent variables. RSM aims at approximating f by a suitable polynomial in some region of the independent process variables. A higher-order polynomial, such as quadratic model may be expressed as [31];

$$Y = \beta_0 + \sum_{i=1}^{n} \beta_i X_i + \sum_{i=1}^{n} \beta_{ii} X_1^2 + \sum_{i=1}^{n} \sum_{j=1}^{n} \beta_{ij} X_i X_j + e \quad (2)$$

where Y is the predicted response, β_0 the constant coefficient, β_i the linear coefficients, β_{ii} the quadratic coefficients, β_{ij} the interaction coefficients, and X_i, X_j are the coded values of the independent process variables, and e is the residual error.

The response surface modeling helps to investigate the response over the entire variables space and to identify the region where it reaches its optimum value.

2.2. Materials

All reagents and chemicals used in the study were of AR grade. Crystal violet dye, N-[4-[bis(4-dimethylamino)-phenyl]-methylene]-2,5-cyclohexadine-1-ylidine]-N-methylmethanaminium chloride (aq. solubility 16 g/l; purity 80%) was procured from M/s Qualigens, India and used without purification. The chemical structure and some characteristics of the dye [20] are given in Fig. 1.

The stock solutions of the dye were prepared by dissolving the desired amount of the crystal violet in double distilled water. The pH of the test solution was adjusted using reagent grade dilute hydrochloric acid and sodium hydroxide.

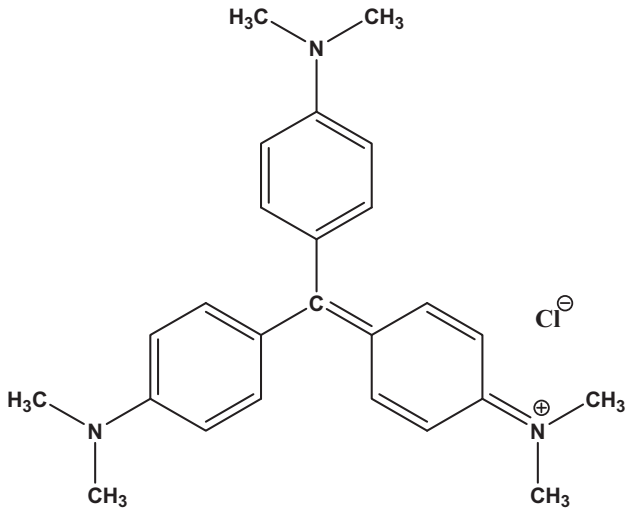

C. I. 42555; λ_{max} 586nm; $C_{25}H_{30}N_3Cl$; Molecular weight 408

Fig. 1. Chemical structure of crystal violet dye.

2.3. Adsorbent development

A magnetic carbon-iron oxide nanocomposite was developed using the activated carbon derived from the coconut shell, an agro waste material. The adsorption features of the activated coconut shell carbon (CSC) and the magnetic properties of iron oxide were combined in a composite to produce magnetic adsorbent. Method for preparation of the CSC is described elsewhere [32]. The prepared CSC was washed thoroughly with double distilled water and dried at 110 °C. For the preparation of magnetic adsorbent, 10 ml of 10 M sodium hydroxide solution was added drop wise to a suspension of CSC (10 g) in 30 ml aqueous solution of ferric nitrate (10 g) to precipitate the iron oxide. The precipitated material was then agitated at 30 °C for 6 h, filtered and calcinated at 750 °C for 1 h. The material was then washed thoroughly with double distilled water and dried at 60 °C. The product was sieved to the desired particle size and finally, stored in vacuum desiccators until required [33].

2.4. Process variables and experimental design

A set of four process variables, viz. initial concentration of the dye (C_0), initial pH of the solution (pH), adsorbent dose (D), and the operating temperature (T) were identified to investigate their influence on the adsorption capacity (mg/g) of prepared magnetic nanocomposite for removal of the crystal violet dye from aqueous solution.

A central composite design (CCD) approach was adopted to decide the number of the sorption experiments to be performed for optimization of the process variables. For a design of four independent variables, the total number of experiments (N) was worked out as 30. Here, this includes the standard 2^n factorial points with their origin at the center, $2n$ axial points fixed at a distance, α from the center to generate the quadratic terms, and n_c replicate points at the center [29]. After having defined the range of each of the process variables, they are coded to lie at ± 1 for the factorial points, 0 for the center points and $\pm\alpha$ for the axial points. The numerical values of the variables were transformed in to their respected coded values as [34];

$$\boldsymbol{Z}_i = \frac{X_i - X_0}{\Delta X_i} \tag{3}$$

where z_i is the dimensionless coded value of the ith independent variable, X_i is the uncoded value of the ith independent variable, X_0 is the uncoded ith independent variable at the center point, and ΔX_i is the step change value. The selected process variables with their limits, units and notations are given in Table 1. Stability of the dye (CV) was ensured at the extremes of the pH and temperature conditions selected for the study.

2.5. Sorption procedure

Batch experiments based on CCD were conducted at random to study the effect of the pre-selected four operating variables on the dye adsorption capacity of the magnetic composite. For sorption of the dye on developed magnetic adsorbent, different weighted amounts of the adsorbent (1–5 g/l) were equilibrated with 50 ml of solution initially containing 240–400 mg/l of the dye. The working standard solutions of the dye were prepared by diluting the stock solution and their pH were adjusted (2.5–8.5) precisely using dilute hydrochloric acid or sodium hydroxide. The sorption experiments were conducted in a thermo-controlled (±1 °C) water bath shaker for 135 min at 120 rpm at different temperatures (10–50 °C). The experimental ranges of the operating temperature and initial pH of the solution were chosen on the basis of existing environmental conditions and our previous findings [32]. The contact time and other conditions were selected on the basis of the results obtained for the preliminary experiments. The equilibrated samples were taken out and the aqueous solution phase was separated from the adsorbent using a centrifuge to make it adsorbent free. The residual concentration of the dye in the solution was then determined using the UV–visible spectrophotometer at 586 nm (λ_{max} of the dye). The adsorption capacity (mg/g) of the adsorbent was calculated as [32];

$$q_e = \frac{(C_0 - C_e)V}{W} \tag{4}$$

where C_0 and C_e are the initial and final concentrations (mg/l) of the dye in solution, respectively. The V and W represent the solution volume (L) and adsorbent weight (g), respectively. All sorption experiments were performed in duplicate and the mean of the two are taken for all calculations. The experimental conditions and the corresponding dye adsorption (mg/g) as measured through the batch experiments are given in Table 2.

2.6. Analytical methods

The pH of the prepared adsorbent was measured after stirring 1.0 g of the nanocomposite with deionized water (100 mL, pH 6.8) for 2 h. The pH at the potential of zero charge (pH_{ZPC}) of the carbon/iron oxide nanocomposite was measured to investigate the

Table 1
Process control variables and their limits.

Variable	Unit	Notation	Limits				
			−2	−1	0	+1	+2
Temperature	°C	T	10	20	30	40	50
Initial pH of solution	–	pH	2.5	4	5.5	7	8.5
Adsorbent dose	g/l	D	1	2	3	4	5
Initial concentration of dye	mg/l	C_0	240	280	320	360	400

Table 2
Central composite design (CCD) for four independent variables (coded values) and corresponding dye adsorption (mg/g).

S no	CCD term	No. of experi-ments	Process variables (coded values)				Adsorption (mg/g)
			T	pH	C_0	*D*	
1	Factorial (2^n)	16	−1, +1	−1, +1	−1, +1	−1, +1	43.4–84.1
2	Axial ($2n$)	8	−2, 0, +2	−2, 0, +2	−2, 0, +2	−2, 0, +2	48.4–85.2
3	Center (n_c)	6	0	0	0	0	61.7–62.3

surface charge of the adsorbent. The pH_{ZPC} was determined using the pH drift method [35]. Initial pH of the series of 0.1 M KCl solutions was adjusted between 2 and 12 using sodium hydroxide or hydrochloric acid. Nitrogen gas was bubbled through the solutions at 25 °C to remove any dissolved CO_2 until the initial pH stabilized. Adsorbent (50 mg) was then added to 50 ml of the KCl solutions maintained at different pH. Final pH of the solutions was measured after 24 h. pH_{ZPC} of the adsorbent was determined form the plot of initial and final pH values of these solutions. The pH of the test solution was adjusted using reagent grade dilute hydrochloric acid and sodium hydroxide. The pH measurements were made using a pH meter (Model 744, Metrohm, Switzerland).

The chemical constituents of the prepared magnetic composite were determined following the methods reported elsewhere [36]. The elemental analysis was performed using the Elemental Analyzer model Vario EL-III (Hanau, Germany). The detection limit for C, H, and N were between 0.1 and 1.0 μg. The iron content of the prepared magnetic adsorbent was determined by atomic absorption spectrophotometer (Perkin Elmer model Analyst-300, USA).

The BET specific surface area (S_{BET}), pore volume (micropore volume, V_{mi}; and total pore volume, V_T), and pore size distribution of the prepared magnetic adsorbent were determined by N_2-physisorption using the surface area analyzer model Autosorb-1C (Quantachrome, USA). The multipoint Brunauer, Emmett, and Teller (BET) surface area was determined from the nitrogen adsorption/desorption isotherm. The BET isotherm equation is typically applied on the adsorption isotherm in P/P0 range of 0.05–0.35. Prior to the measurement, the sample was degassed at 100 Å °Cfor 8 h in an out-gassing station to remove any adsorbed water or entrapped gases in the sample.

Solid phase analysis was conducted by an X-ray Diffractometer (Panalytical X-pert Pro) at 40 kV and 40 mA. The instrument used copper Kα radiation (λ = 1.54 Å) to produce X-rays with a wavelength of 1.54060 Å. Sample was placed in a zero background metal holder and was scanned from 10° to 80° 2θ at a rate of 2° 2θ per min. This scan range covered all major species of iron. The mean diameter, *D*, of the crystallites of the particles was estimated from the pure X-ray diffraction broadening, β, by the Scherrer formula [37];

$$D = \frac{K\lambda}{\beta \cos\theta}$$

where *K* is a constant, approximately equal to unity and related to the crystallite shape and to the way in which β and *D* are defined; λ and θ are the radiation wave-length and Bragg angle, respectively.

Scanning electron microscopy (SEM) was used to investigate the surface topography of the developed adsorbent using the SEM model LEO 430 (Cambridge, England). Samples were set in epoxy and were placed in the sample chamber and evacuated to high vacuum (5×10^{-7} Torr). The sample is bombarded with a finely focused electron beam. A three dimensional topographic image (SEM micrograph) is formed by collecting the secondary electrons generated by the primary beam [38].

The identification of various forms of different constituents in the magnetic adsorbent was done with the help of IR spectra [39]. The IR spectrum was recorded using the Perkin Elmer FTIR model RX1 (USA) in the range 4000–450 cm^{-1}.

The stability of the prepared magnetic nanocomposite was ensured at extreme acidic pH condition (pH 2) as selected for this study. A known amount of the adsorbent was kept for 24 h in acidic (pH 2) solution. The solution was filtered and iron content was determined in the liquid phase after acid digestion using AAS.

Absorbance measurements were made on a Perkin Elmer UV–visible spectrophotometer model Lambada-35. Absorbance values were recorded at the wavelength for maximum absorbance (λ_{max}), i.e. 586 nm for the crystal violet dye. The concentration of the dye was measured with a 1-cm light-path cell, with an absorbance accuracy of ±0.004 at λ_{max}.

2.7. Quadratic polynomial regression modeling

The response variable, *Y* (adsorption capacity, mg/g) of the magnetic composite for the dye in aqueous solution can be expressed as; $Y = f(X_T, X_{pH}, X_{Co}, X_D)$, where, X_T, X_{pH}, X_{Co}, and X_D are the coded values of the process variables (temperature, pH of solution, dye concentration, and adsorbent dose) The selected relationship being a second degree response surface expressed as below [34];

$$Y = \beta_0 + \beta_1 X_T + \beta_2 X_T^2 + \beta_3 X_{pH} + \beta_4 X_{pH}^2 + \beta_5 X_{Co} + \beta_6 X_{Co}^2 + \beta_7 X_D + \beta_8 X_D^2 + \beta_9 X_T X_{pH} + \beta_{10} X_T X_{Co} + \beta_{11} X_T X_D + \beta_{12} X_{pH} X_{Co} + \beta_{13} X_{pH} X_D + \beta_{14} X_{Co} X_D \quad (5)$$

The model coefficients (β_i) are estimated and used for predicting the response values for different combinations of the coded values of the variables.

The adequacy of the selected model and statistical significance of the regression coefficients were tested using the analysis of variance (ANOVA) and the *t*-test statistics [40]. The measured and the model predicted values of the response variable (*Y*) were used to compute the correlation coefficient (R^2), the root mean square error of prediction (RMSEP) and the relative standard error of prediction (RSEP). The correlation between the measured and predicted values indicates the goodness of fit of the model, whereas, the RMSEP and RSEP values are used to evaluate the predictive ability of the selected model [41]. The RMSEP and RSEP were computed as [41];

$$\text{RMSEP} = \sqrt{\frac{\sum_{i=1}^{N}(y_{\text{pred},i} - y_{\text{meas},i})^2}{N}} \quad (6)$$

and

$$\text{RSEP} = \sqrt{\frac{\sum_{i=1}^{N}(y_{\text{pred},i} - y_{\text{meas},i})^2}{\sum_{i=1}^{N}(y_{\text{meas},i})^2}} \times 100 \quad (7)$$

where $y_{pred,i}$ and $y_{meas,i}$ represent the model predicted and measured values of the variable, *Y* and *N* represents the number of experimental observations. The response surface modeling was performed using the Statistica 8.0.

2.8. Model validation and process optimization

The model validation was performed through generating several sets of different combinations of the independent process vari-

ables (temperature, pH, initial dye concentration, adsorbent dose) each within their experimental ranges at constant contact time and agitation speed and corresponding response variable values (adsorption, mg/g) were generated using the model equation after having transformed the process variables to their respective coded values using Eq. (3). Batch experiments were conducted to determine the response variable under fixed conditions of all the process variables for each defined validation set. The model predicted and the experimental values of the response variable for validation set were used to compute the correlation coefficient (R^2), the root mean square error of prediction (RMSEP) and the relative error of prediction (RSEP). The developed quadratic model was finally used to optimize the process variables within their studied experimental ranges. Optimization was performed in Microsoft Excel 97.

2.9. Statistical analysis

The significance of the independent variables and their interactions were tested by means of the analysis of variance (ANOVA). Results were assessed with various descriptive statistics such as *t*-ratio, *p*-value, *F*-value, degrees of freedom (df), correlation coefficient (R^2), adjusted correlation coefficient (R^2_{adj}), sum of squares (SS), mean sum of squares (MSS), and chi-square (X^2) test to reflect the statistical significance of the quadratic model. For the validation of the quadratic model, a non-parametric Mann–Whitney *U*-test and a parametric two-sample (unpaired) *t*-test were conducted to evaluate the relationship between the validation data and the corresponding model predicted responses.

3. Results and discussion

3.1. Characterization of the adsorbent

The pH and pH_{ZPC} of the prepared magnetic nanocomposite were determined as 7.65 and 7.0, respectively. At solution $pH < pH_{ZPC}$, the number of negative charged sites on the adsorbent surface decreases and the positively charged sites increases, whereas, at $pH > pH_{ZPC}$, number of the negatively charged sites on adsorbent surface increases. The elemental analysis of the prepared magnetic adsorbent revealed its chemical constituents as: C 54.31%, H 1.97%; N 0.31%. The atomic absorption spectrophotometric measurement determined the total iron content of the prepared carbon/iron oxide nanocomposite as 9.47%. The result of the stability check of the magnetic adsorbent in acidic medium (pH 2.5) revealed that about 12.4% of the total iron content (94.7 mg/g) of the adsorbent dissolved and leached to the acidic solution at the lowest experimental pH 2.5. The specific surface area of the adsorbent was evaluated from the N_2 isotherms by applying the Brunaeur, Emmett and Teller (BET) equation and was found 335 $m^2\ g^{-1}$. The S_{BET} area of the magnetized nanocomposite was lower than its normal precursor (CSC), which measured 380 $m^2\ g^{-1}$ [32]. This decrease in the surface area of the magnetic nanocomposite as compared with its precursor CSC may be attributed to the formation of iron oxide nanoparticles inside the pores. A similar trend has been observed by others [16,19]. The total and micro pore volumes of the composite were determined as 0.234 and 0.198 cm^3/g, respectively, and the average pore diameter was 2.78 nm. Fig. 2 illustrates the X-ray diffractogram (XRD) of the prepared magnetic nanocomposite in the 2θ range of 10–80°. Six narrow peaks at 2θ values of 30.07, 35.44, 43.16, 54.65, 57.14, and 62.67 indicate that the adsorbent is crystalline in nature [37]. The calculated crystallite sizes (diameter) computed by the Scherrer's equation were found to be in the range of 10.6–19.80 nm. Since the carbon is amorphous in nature, the observed crystallinity of the magnetic nanocomposite originated due to the iron oxide [33].

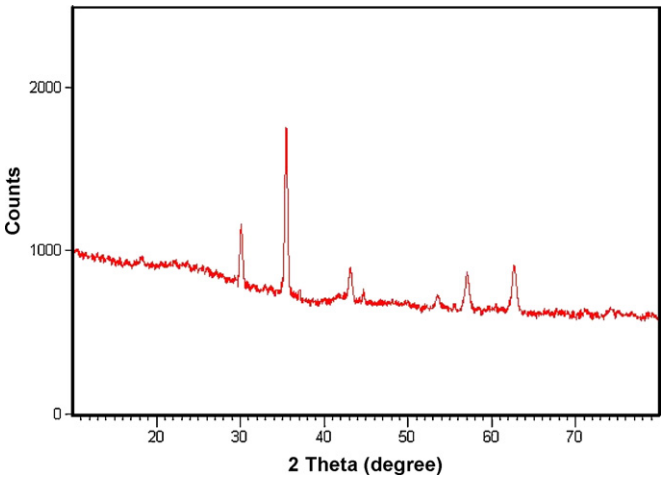

Fig. 2. XRD spectra of the prepared magnetic nanocomposite.

In the present study, scanning electron microscopic (SEM) photograph of the magnetic adsorbent revealed the surface texture, porosity and fibrous structure of the developed nanocomposite (Fig. 3). The surface micrograph showed a distinct roughness pattern with distinct carbon and iron oxide particles, which appear brighter (Fig. 3a). Fig. 3b shows details of the iron oxide particle in nanocomposite. The coarse and rough morphology of the composite could provide more reactive sites than the smooth morphology, and thereby, was in favour of the sorption of dye from aqueous solution [42].

Different constituents in developed carbon-iron oxide nanocomposite were identified with the help of IR spectra [39]. The IR spectrum of the developed adsorbent (Fig. 4) showed weak and broad peaks in the region of 3874–453 cm^{-1}. Approx-

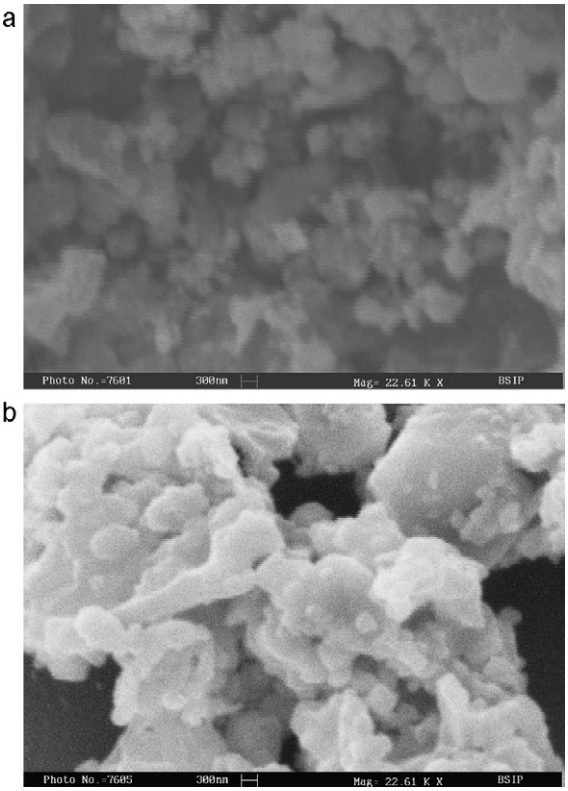

Fig. 3. Scanning electron micrograph (SEM) of the prepared magnetic nanocomposite.

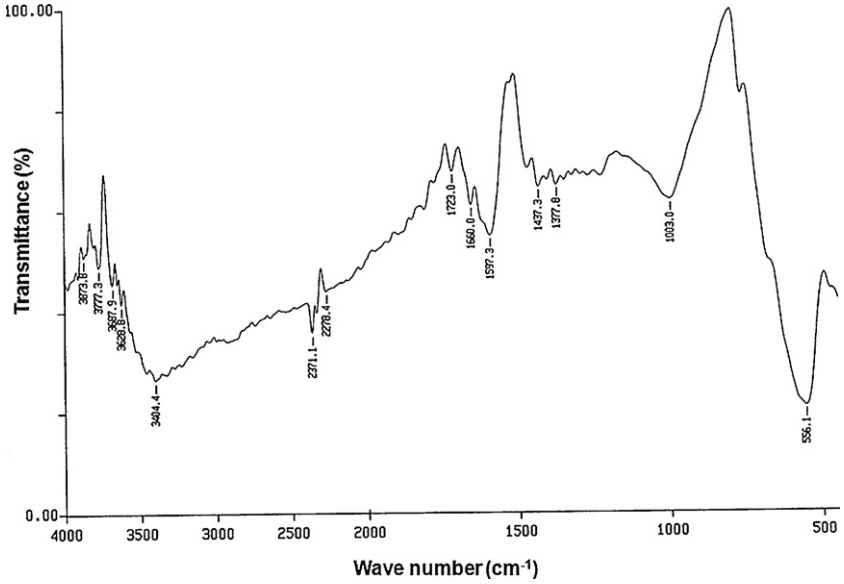

Fig. 4. FT-IR spectra of the prepared magnetic nanocomposite.

imate FT-IR band assignment indicated the presence of carbonyl, carboxyls, lactones, phenols, olefinic and aromatic structures. The broad band at 3404.4 cm^{-1} represented –OH group. The 1800–1540 cm^{-1} bands are associated with C=O stretching mode in carbonyls, carboxylic acids, and lactones and C=C bonds in olefinic and aromatic structures, whereas the 1440–1000 cm^{-1} band was assigned to the C–O and O–H bending modes. The assignment of a specific wave number to a given functional group was not possible because the absorption bands of various functional groups overlap and shift, depending on their molecular structure and environment. Shifts in absorption positions can be caused by the factors such as intra-molecular and intermolecular hydrogen bonding, steric effects, and degrees of conjugation [39].

A contact of the magnet with the water suspension containing the prepared carbon/iron oxide nanocomposite immediately led to aggregation of all the particles collected on the inner surface of the container opposite the magnet (figure not shown due to brevity) and the clear (particles free) solution could be easily decanted off. This suggests that the prepared nanocomposite possessed magnetism and could be potentially used as a magnetic adsorbent to remove the compounds in liquid phase.

3.2. Response surface modeling

3.2.1. Experimental design and quadratic model

CCD approach was adopted for investigating the individual and interactive effects of the selected process variables on the adsorption of dye by the developed magnetic nanocomposite from aqueous solution. The maximum adsorption capacity of the composite for CV dye was observed to be 85.20 mg/g. Polynomial regression modeling was performed between the response variable and the corresponding coded values (X_T, X_{pH}, X_{Co}, X_D) of the four different process variables, and finally, the best fitted model equation was obtained as;

$$Y\,(\mathrm{mg/g}) = 62.58 + 9.06X_T + 0.97X_T^2 + 2.10X_{pH} - 0.13X_{pH}^2 - 0.22X_{Co} - 0.48X_{Co}^2 - 4.52X_D - 0.01X_D^2 - 0.18X_TX_{pH} - 2.05X_TX_{Co} - 0.79X_TX_D - 2.08X_{pH}X_{Co} + 1.27X_{pH}X_D + 0.92X_{Co}X_D \quad (8)$$

The model equation (8) was used to evaluate the influence of process variables on the response factor, the dye adsorption (mg/g) from aqueous solution by the developed magnetic composite. The analysis of variance (ANOVA) is considered to be essential to test the significance of the model [34]. The ANOVA results (Table 3) of the quadratic regression model (Eq. (8)) suggest that the model was highly significant, as evident from the Fisher's *F*-test (F_{model} = 145.34) with a very low probability value (p_{model} = 0.000). Furthermore, the calculated *F*-value (F_{model} = 145.34) was compared with the critical *F* value ($F_{0.05,df,\ (n-df+1)}$) for the considered probability (p = 0.05) and degrees of freedom. Since, the df for model are 14 and n = 30, it gives (n − df + 1) = 15. The critical *F* value ($F_{0.05,14,15}$ = 2.42) is less than the calculated *F*-value of 145.34. It suggests that the computed Fisher's variance ratio at this level was large enough to justify a very high degree of adequacy of the quadratic model and significance of the variables combinations [34,40,43].

The goodness of fit of the model was checked by the correlation coefficient (R^2) between the experimental and model predicted values of the response variable (Fig. 5a).

A fairly high value of R^2 (0.993) indicated that most of the data variation was explained by the regression model. Moreover, a closely high value of the adjusted correlation coefficient (R_a^2 = 0.986) also showed a high significance of the model. The R_{adj}^2 corrects the R^2 value for the sample size and the number of terms in the model. If there are many terms in the model and the sample size is not very large, the R_{adj}^2 may be noticeably smaller than the R^2. In our case the, the values of R_{adj}^2 and R^2 were found to be very close. A similar pattern has been reported by others for the second order RSM experiments based on central composite [43] and Box Benhken [40] designs. Further, a considerably low RMSEP (0.91) and RSEP (1.43) values suggest for the adequacy of the fitted quadratic model. The chi-square (χ^2) test was also performed to check whether there was a significant difference between the model responses and the observed data. The calculated chi-square value ($\chi_{cal}^2 = 0.34$) was found to be less than the critical value ($X_{crit}^2 = 42.56$) suggesting that there was no significant difference between the observed and the expected responses. The chi-square (χ^2) test concluded with 95% certainty that the quadratic model provided a satisfactory fit to the experimental data.

Table 3
Analysis of variance (ANOVA) of the response surface quadratic model for the prediction of crystal violet dye adsorption efficiency.

Source	Sum of squares	DF[a]	Mean sum of squares	*F*-value	*p*-value	Remark
Model	2766.57	14	197.61	145.34	0.000000	Significant
X_T	1800.90	1	1800.90	1323.97	0.000000	Significant
X_{pH}	96.41	1	96.41	70.90	0.000000	Significant
X_{C_0}	1.08	1	1.08	0.79	0.387566	
X_D	469.83	1	469.83	338.19	0.000000	Significant
X_T^2	27.28	1	27.28	20.06	0.000441	Significant
X_{pH}^2	0.52	1	0.52	0.38	0.545069	
$X_{C_0}^2$	6.83	1	6.83	5.02	0.040552	Significant
X_D^2	0.00	1	0.00	0.00	0.868735	
$X_T * X_{pH}$	0.45	1	0.45	0.33	0.572327	
$X_T * X_{C_0}$	66.63	1	66.63	49.01	0.000004	Significant
$X_{pH} * X_{C_0}$	68.68	1	68.68	50.51	0.000004	Significant
$X_T * X_D$	9.89	1	9.89	7.28	0.016548	Significant
$X_{pH} * X_D$	25.50	1	25.50	18.75	0.000594	Significant
$X_{C_0} * X_D$	12.44	1	12.44	9.15	0.008531	Significant
Error	20.40[b]	15	1.36[c]			
Total	2786.96	29				

[a] DF-degrees of freedom.
[b] SS_E.
[c] MSS_E.

A plot of the normal probability of the residuals is shown in Fig. 5b. The normal probability plot of the residuals is an important diagnostic tool to detect and explain the systematic departures from the assumption that errors are normally distributed and is independent of each other, and that the error variance is homogeneous. Information regarding the lack of fit of the selected model is contained in the residuals [43]. The normal probability of the residuals (Fig. 5b) suggests that almost no serious violation of the assumptions underlying the analyses and it confirmed the normality assumptions and independence of the residuals. Moreover, the comparison of the residuals with the error variance showed that none of the individual residual exceeded the value twice of the square root of the error variance [34].

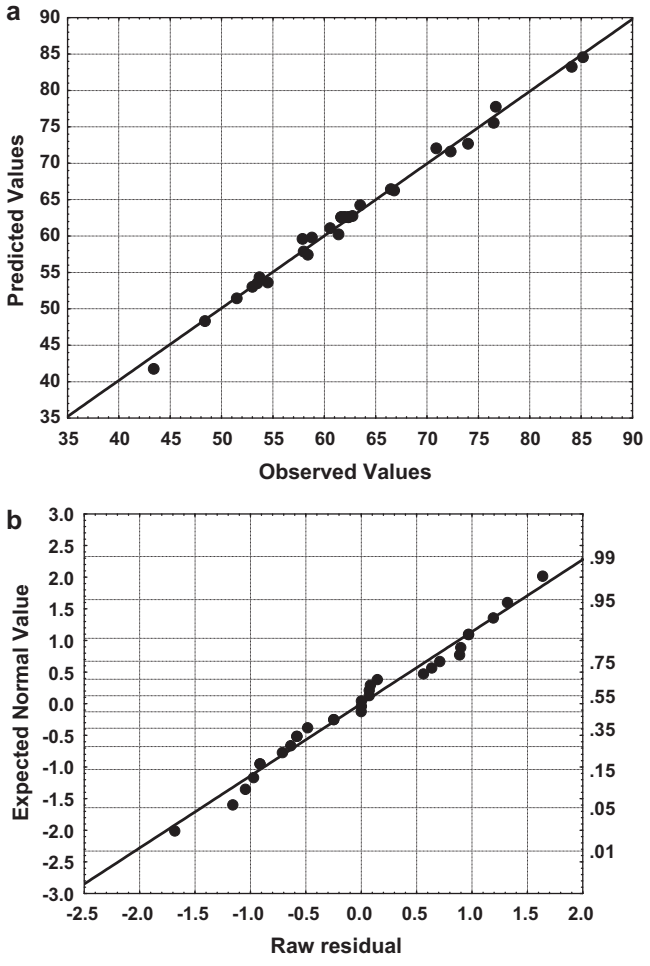

Fig. 5. (a) Plot of the measured and model predicted values of the response variable and (b) the normal probability plot of the raw residuals.

3.2.2. *Effects of model components and their interactions on dye adsorption*

The significance of the quadratic model coefficients was evaluated by the Student's *t*-test and *p*-values listed in Table 4. The *t*-value is the ratio of the estimated parameter effect and the estimated parameter standard deviation. The parameter effect is estimated as twice the regression coefficient value for that parameter. The *p*-value is used as a tool to check the significance of the coefficient. The larger the magnitude of the *t*-value and the smaller the *p*-value, the more significant is the corresponding parameter in the regression model [44].

From Table 4, it is evident that all the linear (except C_0) and quadratic (except pH and D) terms are statistically significant ($p < 0.05$). Among the interactive terms, except the interaction of pH with temperature (pH*T), all interactions are statistically significant. The statistical results (Table 3) further suggested that the temperature (T), the adsorbent dose (D), and the solution pH are among the variables exhibiting most significant effect on the adsorption of the dye. Moreover, the first-order main effects of all the four independent variables viz. temperature (X_T), initial pH of solution (X_{pH}), initial dye concentration (X_{C_0}), and the adsorbent dose (X_D) were found to be more significant than their respective quadratic effects (X_T^2, X_{pH}^2, X_{Co}^2, and X_D^2). The *t*- and *p*-value (Tables 3 and 4) suggest that the temperature, dose and initial pH of the solution have a direct relationship on the dye adsorption efficiency of the developed nano-composite. It may be noted that temperature was the most significant component of the regression model for the present application, whereas, the quadratic dose term showed the lowest effect on the dye adsorption efficiency.

For the regression coefficients, both the magnitude and sign are important, as the earlier indicates the importance or influence of the variable on the response factor, whereas, the sign determines its effect direction. A positive sign of the coefficient represents a synergistic effect, while a negative sign indicates an antagonistic effect. The adsorbent dose, initial dye concentration and the interactive terms viz. $X_T * X_{pH}$, $X_T * X_{Co}$, $X_{pH} * X_{Co}$, and $X_T * X_D$ along with the

Table 4
Multiple regression results and significance of the components for the quadratic model.

Factor (coded)	Parameter	Coefficient	Effect	*t*-value	Sum of squares	PC
Intercept	β_0	62.580	125.160	142.463	0.000	
X_T	β_1	9.059	18.118	36.386	0.000	69.89
X_{pH}	β_3	2.096	4.193	8.420	0.000	3.74
X_{C_0}	β_5	−0.219	−0.438	−0.890	0.388	0.04
X_D	β_7	−4.523	−9.046	−18.390	0.000	17.85
X_T^2	β_2	0.966	1.933	4.479	0.000	1.06
X_{pH}^2	β_4	−0.134	−0.267	−0.619	0.545	0.02
$X_{C_0}^2$	β_6	−0.484	−0.967	−2.241	0.041	0.27
X_D^2	β_8	−0.009	−0.017	−0.040	0.969	0.00
$X_T * X_{pH}$	β_9	−0.175	−0.351	−0.577	0.572	0.02
$X_T * X_{C_0}$	β_{10}	−2.048	−4.097	−7.000	0.000	2.59
$X_{pH} * X_{C_0}$	β_{12}	−2.080	−4.159	−7.107	0.000	2.67
$X_T * X_D$	β_{11}	−0.789	−1.578	−2.697	0.017	0.38
$X_{pH} * X_D$	β_{13}	1.267	2.534	4.330	0.001	0.99
$X_{C_0} * X_D$	β_{14}	0.919	1.838	3.025	0.009	0.48

PC, percent contribution.

quadratic terms of pH (X^2_{pH}), concentration ($X^2_{C_0}$), and adsorbent dose (X^2_D) exhibited negative relationship with the dye adsorption process, whereas, the interactive terms of dose with pH ($X_{pH} * X_D$) and concentration ($X_D * X_{Co}$) showed positive significant effect on the process.

The percent contribution (PC) of each of the individual term in final model were computed (Table 4) using the SS values of the corresponding term. The PC of a term is obtained as the ratio of SS of an individual term to that of sum of SS for all the terms [40], as;

$$\mathrm{PC} = \frac{\mathrm{SS}}{\Sigma \mathrm{SS}} \times 100 \tag{9}$$

As evident from Table 4, the temperature (X_T) showed the highest level of significance with a contribution of >69% as compared to other components..

3.2.3. Model validation

Validation of the quadratic model was performed through generating five sets of different combinations of the four independent process variables in a random fashion [45,46], each within its respective experimental range and corresponding response variable (adsorption, mg/g) was generated using the coded values of the process variables and model equation (8). Experimentally determined response factor values for each of the five set of process variables were then used along with the model predicted values to compute the R^2, RMSEP and RSEP values. The experimental conditions along with the model predicted and experimental results are presented in Table 5. It may be noted that the dye adsorption determined for the validation batch experiments exhibited a variation between 47.48 and 80.68 mg/g. A high correlation ($R^2 = 0.993$) among the predicted and the measured values of the response factor and considerably low RMSEP (1.36) and RSEP (2.05) values suggest for the adequacy of the selected quadratic model in predicting the response variable for the validation data set comprised of different combinations of the process variables.

In order to examine whether the experimental adsorption data in validation set differ from the corresponding model predicted values of the response variable, a non-parametric Mann–Whitney *U*-test was conducted [40], which is based on the combined ranking of the two samples and summing up their total rank scores (U) separately after their break up. An expected score value is determined as [47],

$$E(U) = \frac{n_u(N+1)}{2} \tag{10}$$

where $E(U)$ is the expectation of U, n_U is the sample size of the data set being tested, and N is the total number of samples ($N = n_1 + n_2$). A z-score under the normal curve is then calculated as [48],

$$Z = \frac{U_{\max} - E(U)}{\sqrt{n_1 n_2 (N+1)/2}} \tag{11}$$

where U_{max} is the maximum total rank score value, and n_1 and n_2 are the sample sizes of the two independent data sets. The z-score for the present validation data set was determined to be 0.1206 and the two-tailed probability associated with this z-score was obtained as $p = 0.904$, which is greater than the chosen probability level of $p = 0.05$, suggesting that there was no significant difference between the measured and the model predicted responses in validation set [40].

A parametric two-sample (unpaired) t-test was also performed to evaluate the relationship between the model predicted and the experimental responses [40]. Since, both the predicted and experimental data sets have almost equal variance; the standard error of the two sets can be pooled [48] as;

$$\mathrm{se_p} = \frac{s_1 + s_2}{2} \sqrt{\frac{1}{n_1} + \frac{1}{n_2}} \tag{12}$$

where se_p is the pooled standard error, s_1 and s_2 are the standard deviations, and n_1 and n_2 are the sample sizes of the two data sets.

Table 5
The actual (A) and coded (C) values of the independent process variables in model validation set and corresponding values of the response variable.

Exp. no.	Temp. (°C)		pH		Adsorbent dose (g/l)		Dye concn. (mg/l)		Adsorption (mg/g)	
	A	C	A	C	A	C	A	C	Pred.	Expt.
1	15	−1.5	3	−1.67	1.5	−1.5	260	−1.5	49.42	48.14
2	25	−0.5	4	−1	2	−1	300	−0.5	60.52	58.69
3	30	0	5	−0.33	2.5	−0.5	340	0.5	62.88	64.12
4	35	0.5	6	0.33	3.5	0.5	380	1.5	64.44	65.36
5	45	1.5	8	1.67	4.5	1.5	400	2	70.94	69.72

Pred, model predicted; Expt, experimental.

Table 6
Adsorption capacity (Q^0) of various adsorbents for the crystal violet dye.

Adsorbents	Q^0 (mg/g)	Reference
Phosphoric acid activated carbon (PAAC)	60.42	[5]
Sulphuric acid activated carbon (SAAC)	85.84	[5]
Jute fiber carbon	27.99	[51]
Kaolin	47.27	[52]
Coniferous pinus bark powder (CPBP)	32.78	[20]
Semi-IPN hydrogels	35.09	[2]
Magnetic nanocomposite	81.70 (111.80)	This study (optimum value)

The *t*-test statistics was then applied calculating the t_{cal}-value, as [48];

$$t_{cal} = \frac{\bar{y}_1 - \bar{y}_2}{se_p} \quad (13)$$

where t_{cal} is the calculated *t*-statistics, and $\bar{y}_1$ and $\bar{y}_2$ are the mean values of the independent data sets. The value was compared with the critical *t*-value (t_{crit}) for the corresponding degrees of freedom ($df = n_1 + n_2 - 1$). The calculated *t*-value ($t_{cal} = 0.07$) was found to be less than the critical value of *t* ($t_{crit} = 2.41$), suggesting that there is no significant statistical difference between the two set of independent samples. Therefore, the *t*-statistics concluded with 95% certainty that the proposed quadratic model provided a satisfactory fit to the validation data set [40].

3.2.4. Dye adsorption capacity of the magnetic composite

The dye adsorption capacity (mg/g) of the prepared magnetic nanocomposite was evaluated using the Langmuir sorption isotherm, as [32];

$$\frac{c_e}{q_e} = \frac{1}{Q^0 b} + \frac{c_e}{Q^0} \quad (14)$$

where q_e is the amount of solute adsorbed per unit weight of adsorbent (mg/g), C_e the equilibrium concentration (mg/l), Q^0 the monolayer adsorption capacity (mg/g) and *b* is a constant. The model parameters (Q^0 and *b*) can be determined from the linear plots of C_e/q_e and C_e [32]. The isotherm (figure not shown due to brevity) showed a good fit to the experimental data ($R^2 = 0.91$). The Langmuir adsorption capacity of the magnetic nanocomposite at 50 °C and pH 8.5 was found to be 81.7 mg/g, whereas, that of the non-magnetic adsorbent used as the precursor of the developed magnetic nano-composite was determined as 40 mg/g at 50 °C and pH 8.5. A considerably high value of the adsorption capacity of the developed magnetic nanocomposite towards the removal of the dye from water as compared with the capacity of non-magnetic precursor adsorbent suggests for its usefulness for employing it in dye contamination situations. The adsorption capacities (Q^0) obtained for adsorption of CV dye on to various other adsorbents reported in the literature are listed in Table 6. However, it should be noted that the adsorption characteristics largely depend on many parameters such as particle size, pH of the solution, and the results presented in Table 6 are based on experiments conducted under different operating conditions. Results show that the developed magnetic nanocomposite is a better adsorbent compared to most of the adsorbents used.

3.2.5. Three-dimensional response surface plots

The three-dimensional (3D) response surface plots of the dependent variable as a function of two independent variables, maintaining all other variables at fixed levels can provide information on their relationships and can be helpful in understanding both the main and the interaction effects of these two independent variables [46,49]. Therefore, in order to gain better understanding of the effects of the independent variables and their interactions on the dependent variable, 3D response surface plots for the measured responses were constructed based on the quadratic model. The influence of the four different process variables on the response factor (adsorption, mg/g) are visualized in the 3D response surface plots (Figs. 6 and 7a–c).

Fig. 6a shows the combined effect of temperature and pH on adsorption of the dye at constant concentration (320 mg/l) and adsorbent dose (3 g/l). The dye sorption increases with both the solution pH and temperature within their respective experimental ranges. Such a temperature-dependence may be understood as increase in temperature may enhance the number of binding sites for the dye molecules on the adsorbent surface [23]. The pH dependence of dye adsorption on magnetic composite may be explained in terms of the solution pH and pH_{ZPC} of the adsorbent. At solution pH < pH_{ZPC}, a relatively lower number of negative charged sites on the adsorbent surface do not favour the adsorption of cationic dyes due to the electrostatic repulsion, whereas, at pH > pH_{ZPC}, a relatively higher number of negatively charged sites on adsorbent surface enhances the sorption of dye [50]. A maximum adsorption of dye (>85 mg/g) was determined at constant initial concentration (320 mg/l) and adsorbent dose (3 g/l).

The interactive effect of temperature and initial dye concentration on adsorption at constant pH (5.5) and adsorbent dose (3 g/l) is shown in Fig. 6b. It is evident that adsorption in the experimental range at lower temperature increases with increasing concentration, whereas, the trend reverses at higher temperature where the dye sorption decreases with increasing concentration. This behavior can be understood as the increasing adsorbate concentration with fixed adsorbent dose would result in saturation of the binding sites on the surface at lower temperature and subsequently declining of the adsorbate uptake with increasing concentration, whereas, at higher temperature, the number of binding sites increases, hence enhancing the sorption process. A maximum dye removal (>85 mg/g) was determined at constant pH (5.5) and adsorbent dose (3 g/l).

The combined effect of temperature and adsorbent dose on dye uptake is shown in Fig. 6c. It may be noted that the dye sorption increases with temperature and decreases with increasing dose within the experimental range. The observed trend may be understood that the increase in dose would make higher number of adsorption sites available, which against a constant dye concentration would result in lowering of the concentration gradient between the solution bulk and the adsorbent interface, resulting into declining adsorption rate. Whereas, for the low adsorbent dose, the concentration gradient will be relatively high, resulting in higher adsorption rate. A maximum dye removal (>85 mg/g) was observed at constant pH (5.5) and dye concentration (320 mg/l).

Fig. 7a shows the interactive influence of pH and initial concentration of the dye on adsorption from the aqueous phase. It is evident that the dye uptake increases with the increase in both the pH and the dye concentration. A maximum dye uptake is observed at pH 8.5, which may be explained in terms of the solution pH and pH_{ZPC} of the adsorbent. A maximum dye removal (>66 mg/g) was observed at constant temperature (30 °C) and adsorbent dose (3 g/l).

The plot for combined effect of the solution pH and adsorbent dose (Fig. 7b) suggests that the dye uptake by the adsorbent decreases with increasing dose and increases with the solution pH. Such a pattern of the dye sorption may be explained in terms of the solution pH and pH_{ZPC} of the composite, which attains reversal of charge density below and above its zero point charge pH. A maximum dye uptake is observed at pH 8.5 and adsorbent dose of 3 g/l. A maximum dye removal (>73 mg/g) was observed at constant temperature (30 °C) and initial dye concentration (320 mg/l).

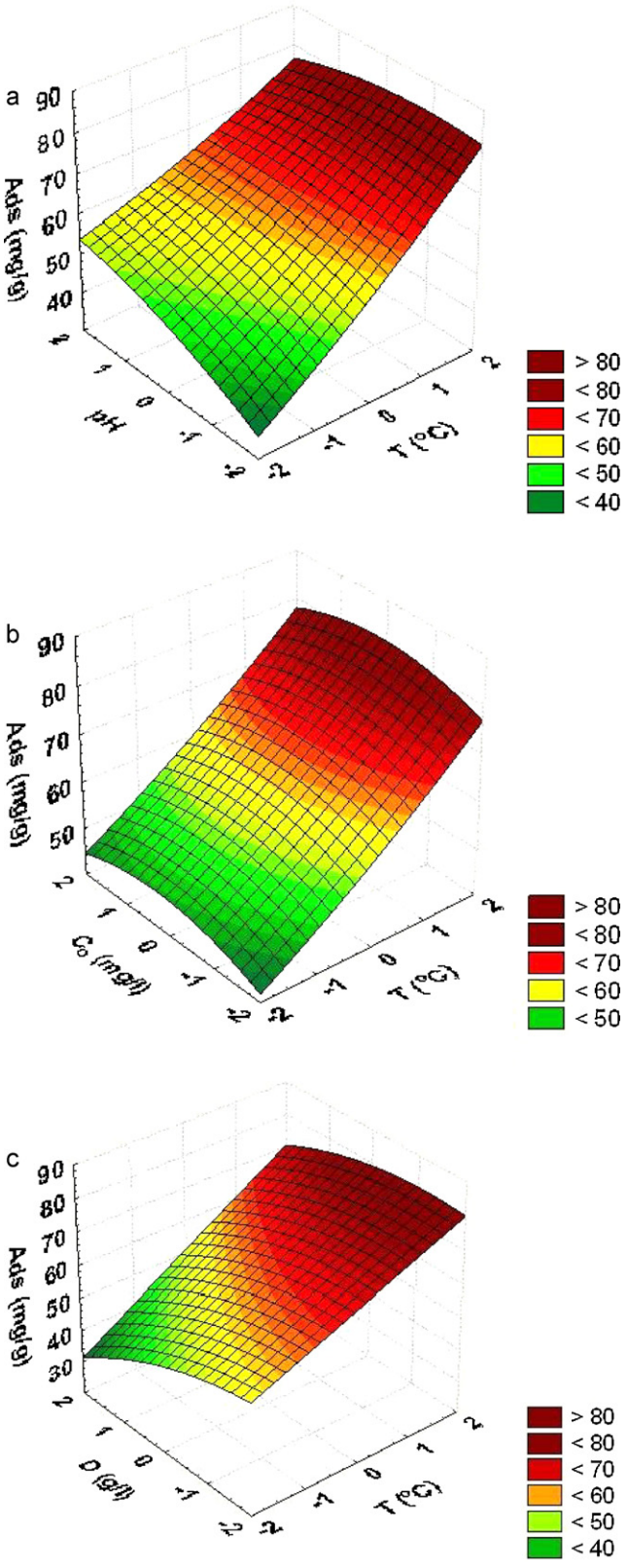

Fig. 6. The 3D plots showing effect of (a) temperature and pH, (b) temperature and initial concentration of the dye, and (c) temperature and adsorbent dose on adsorption of the crystal violet dye.

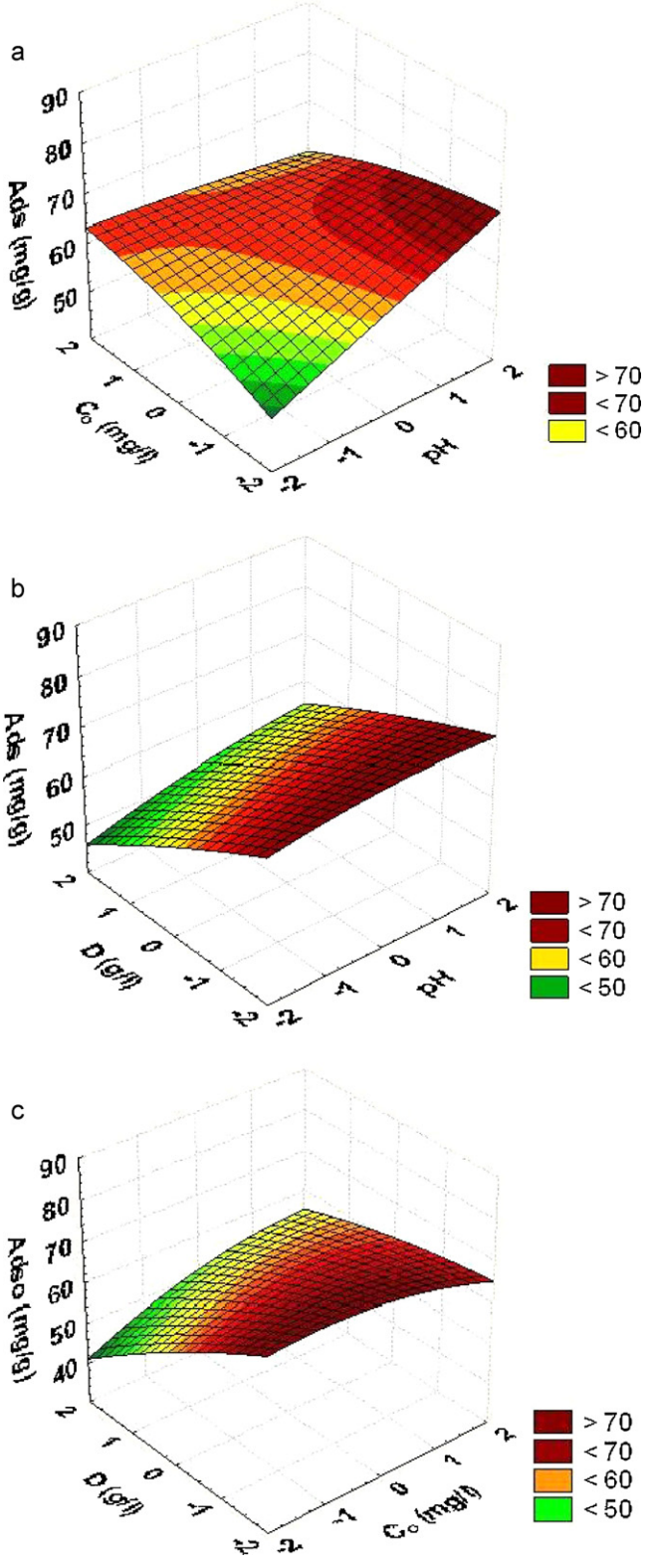

Fig. 7. The 3D plots showing effect of (a) pH and initial concentration of dye, (b) pH and adsorbent dose, and (c) initial concentration of dye and adsorbent dose on adsorption of the crystal violet dye.

The combined effect of adsorbent dose and dye concentration on dye uptake by the adsorbent is visible in Fig. 7c. It may be seen that increasing dose level results in an decreasing adsorption of the dye, whereas, it increases with the dye concentration. An optimum dye uptake is observed at the lowest adsorbent dose and highest dye concentration. At constant temperature (30 °C) and dose (3 g/l), a maximum dye removal of >73 mg/g was determined.

3.2.6. Optimization of the dye adsorption

The process optimization modeling suggested the optimum values of different independent process variables as; the initial dye concentration 240 mg/l; temperature 50 °C; initial solution pH 8.5; and the adsorbent dose 1 g/l, to achieve the maximum adsorption (113.31 mg/g) of the CV dye. The corresponding experimental value of the dye adsorption under the optimum condition of the variables was determined as 111.80 ± 1.42 mg/g (mean ± SD of three replicates), which is very close to the optimized value. The optimum value of the dye adsorption is much higher than the Langmuir monolayer adsorption capacity (81.70 mg/g) of the developed magnetic composite determined in the experimental data range.

4. Conclusions

The developed magnetic nanocomposite was found superior than its precursor carbon exhibiting higher adsorption capacity for removal of the crystal violet dye from aqueous solution. The adsorption capacity of the non-magnetic carbon and the developed magnetic nanocomposite were 40 mg/g and 81.7 mg/g, respectively, in the experimental range of the variables. The application of a CCD combining with the RSM and optimization helped in reaching the global optimal solution for maximizing the dye adsorption from aqueous solution by the developed magnetic nanocomposite. The proposed mathematical approach also provided a critical analysis of the individual and simultaneous interactive influences of the selected independent variables, such as the initial dye concentration, initial pH of the solution, adsorbent dose and the operating temperature on the adsorption process of the crystal violet dye. For the optimum values of the process variables, the predicted dye adsorption on to the nanocomposite was 113.31 mg/g.

The model predicted values of the response variable were in very good agreement with the experimentally determined values ($R^2 = 0.993$, RMSEP = 0.91, RSEP = 1.43). The statistical analysis results suggested that the first-order main effects of the independent variables (X_{pH}, X_{Co}, X_T, and X_D) were relatively more significant than their respective quadratic effects on the dye removal capacity of the composite. Temperature was the most significant component of the quadratic model for the present adsorbent-adsorbate system ($t = 36.386$, $p = 0.000$, $F = 1323.97$, PC = 69.97).

The model validation results suggested for the adequacy of the developed model ($R^2 = 0.993$, RMSEP = 1.36, RSEP = 2.05) for its application to new data sets. The results clearly confirmed that the proposed four-factor CCD combined with RSM and optimization is an effective approach for modeling the sorption process of the crystal violet dye to understand the relationships among the independent and response variables and to maximize the process efficiency. The developed magnetic nanocomposite may be used for removal of cationic basic dye from water.

Acknowledgements

The authors thank the Director, Indian Institute of Toxicology Research, Lucknow (India) for his keen interest in this work. Special thanks are due to Prof. Nishith Verma, and Dr. Dinesh Deva, Department of Chemical Engineering, IIT, Kanpur (India) for helping in XRD and surface area measurements of the adsorbent.

References

[1] O.J. Hao, H. Kim, P.C. Chiang, Decolorization of wastewater, Environ. Sci. Technol. 30 (2000) 449–505.
[2] S. Li, Removal of crystal violet from aqueous solution by sorption into semi-interpenetrated networks hydrogels constituted of poly (acrylic acid–acrylamide–methacrylate) and amylase, Bioresour. Technol. 101 (2010) 2197–2202.
[3] I. Eiichi, T. Ogawa, T.C. Yatome, H. Horisu, Behavior of activated sludge with dyes, Bull. Environ. Contam. Toxicol. 35 (1985) 729–734.
[4] H. He, S. Yang, K. Yu, Y. Ju, C. Sun, L. Wang, Microwave assisted induced catalytic degradation of crystal violet in nano-nickel dioxide suspensions, J. Hazard. Mater. 173 (2010) 393–400.
[5] S. Senthilkumaar, P. Kalaamani, C.V. Subburaam, Liquid phase adsorption of crystal violet on to activated carbons derived from male flowers of coconut tree, J. Hazard. Mater. 136 (2006) 800–808.
[6] J.J. Jone, J.O. Falkinham III, Decolorization of malachite green and crystal violet by waterborne pathogenic mycobacteria, Antimicrob. Agents Chemother. 47 (2003) 2323–2326.
[7] D. Ghosh, K.G. Bhattacharyya, Adsorption of methylene blue on kaolinite, Appl. Clay Sci. 20 (2002) 295–300.
[8] J. Huang, K. Huang, S. Liu, A. Wang, C. Yan, Adsorption of rhodamine B and methyl orange on a hypercrosslinked polymeric adsorbent in aqueous solution, Colloids Surf. A 330 (2008) 55–61.
[9] B. Gozmen, B. kayan, A.M. Gizir, A. Hesenov, Oxidative degradation of reactive blue 4 dye by different advanced oxidation methods, J. Hazard. Mater. 168 (2009) 129–136.
[10] S. Khansorthong, M. Hunsom, Remediation of waste water from pulp and paper mill industry by the electrochemical technique, Chem. Eng. J. 151 (2009) 228–234.
[11] M.K. Purkait, S. Dasgupta, S. De, Micellar enhanced ultrafiltration of eosin dye using hexadecyl pyridinium chloride, J. Hazard. Mater. 136 (2006) 972–977.
[12] A.N. Kagalkar, U.B. Jagtap, J.P. Jadhav, V.A. Bapat, S.P. Govindwar, Biotechnological strategies for phytoremediation of the sulfonated azo dye direct red 5B using blumea malcolmii hook, Bioresour. Technol. 100 (2009) 4104–4110.
[13] A. Mittal, J. Mittal, A. Malviya, D. Kaur, V.K. Gupta, Adsorption of hazardous dye crystal violet from waste water by waste materials, J. Colloid Interface Sci. 343 (2010) 463–473.
[14] P. Panneer Selvam, S. Preethi, P. Basakaralingam, N. Thinakaran, A. Sivasamy, S. Sivanesan, Removal of rhodamine B from aqueous solution by adsorption onto sodium montmorillonite, J. Hazard. Mater. 155 (2008) 39–44.
[15] L. Ai, H. Huang, Z. Chen, X. Wei, J. Jiang, Activated carbon/$C_0Fe_2O_4$ composite: facile synthesis, magnetic performance and their potential application for the removal of malachite green from water, Chem. Eng. J. 156 (2010) 243–249.
[16] M. Schwickardi, S. Olejnik, E.L. Salabas, W. Schmidt, F. Schuth, Scalable synthesis of activated carbon with superparamagnetic properties, Chem. Commun. (2006) 3987–3989.
[17] C.F. Chang, P.H. Lin, W. Holl, Aluminum-type superparamagnetic adsorbents: synthesis and application on fluoride removal, Colloids Surf. 280 (2006) 194–202.
[18] S.S. Banerjee, D.H. Chen, Fast removal of copper ions by gum arabic modified magnetic nano-adsorbent, J. Hazard. Mater. 147 (2007) 792–799.
[19] N. Yang, S. Zhu, D. Zhang, S. Xu, Synthesis and properties of magnetic $Fe_3O_4^-$ activated carbon nanocomposite particles for dye removal, Mater. Lett. 62 (2008) 645–647.
[20] R. Ahmad, Studies on adsorption of crystal violet dye from aqueous solution onto Coniferous pinus bark powder (CPBP), J. Hazard. Mater. 171 (2009) 767–773.
[21] L.C.A. Oliveira, R.V.R.A. Rios, J.D. Fabris, V. Garg, K. Sapag, R.M. Lago, Activated carbon/iron oxide magnetic composites for the adsorption of contaminants in water, Carbon 40 (2002) 2177–2183.
[22] S. Pirrilo, M.L. Ferreira, E.H. Rueda, Adsorption of Alizarin, Eriochrome blue Black R, and Fluorescein using different iron oxides as adsorbents, Ind. Eng. Chem. Res. 46 (2007) 8255–8263.
[23] J.N. Sahu, J. Acharya, B.C. Meikap, Response surface modeling and optimization of chromium(VI) removal from aqueous solution using tamarind wood activated carbon in batch process, J. Hazard. Mater. 172 (2009) 818–825.
[24] K.P. Singh, P. Ojha, A. Malik, G. Jain, Partial least squares and artificial neural networks modeling for predicting chlorophenol removal from aqueous solution, Chemom. Intell. Lab. Syst. 99 (2009) 150–160.
[25] Z. Alam, S.A. Muyibi, J. Toramae, Statistical optimization of adsorption processes for removal of 2 4-dichlorophenol by activated carbon derived from oil palm empty fruit bunches, J. Environ. Sci. 19 (2007) 674–677.
[26] P. Ricou-Hoeffer, I. Lecuyer, P.L. Cloirec, Experimental design methodology applied to adsorption of metallic ions onto fly ash, Water Res. 35 (2001) 965–976.
[27] U.K. Garg, M.P. Kaur, V.K. Garg, D. Sud, Removal of nickel(II) from aqueous solution by adsorption on agricultural waste biomass using a response surface methodological approach, Bioresour. Technol. 99 (2008) 1325–1331.
[28] I.A.W. Tan, A.L. Ahmad, B.H. Hameed, Optimization of preparation conditions for activated carbons from coconut husk using response surface methodology, Chem. Eng. J. 137 (2008) 462–470.
[29] R.H. Myers, D.C. Montgomery, Response Surface Methodology, second ed., Wiley, 2001.

[30] G. Annadurai, R.S. Juang, D.J. Lee, Adsorption of heavy metals from water using banana and orange peels, Water. Sci. Technol. 47 (2003) 185–190.
[31] M.Y. Can, Y. Kaya, O.F. Algur, Response surface optimization of removal of nickel from aqueous solution by cone biomass of Pinus sylvestris, Bioresour. Technol. 97 (2006) 1761–1765.
[32] K.P. Singh, A. Malik, S. Sinha, P. Ojha, Liquid-phase adsorption of phenols using activated carbons derived from agricultural waste material, J. Hazard. Mater 150 (2008) 626–641.
[33] R. Ahmad, R. Kumar, Kinetic and thermodynamic studies of brilliant green adsorption onto carbon/iron oxide nanocomposite, J. Korean Chem. Soc. 54 (2010) 125–130.
[34] R. Sen, T. Swaminathan, Response surface modeling and optimization to elucidate and analyze the effects of inoculum age and size on surfactin production, Biochem. Eng. J. 21 (2004) 141–148.
[35] Y.F. Jia, B. Xiao, K.M. Thomas, Adsorption of metal ions on nitrogen surface functional groups in activated carbons, Langmuir 18 (2002) 470–478.
[36] Al. Vogel, A Text Book of Quantitative Chemical Analysis, ELBS Publication, London, England, 1991.
[37] F.M. De, Y. Peng, C.T. Hu, H.H. Ping, Y. Aihua, C.K. Min, Z.J. Xi, L. Dong, Synthesis, characterization and size control of zerovalent iron nanoparticles anchored on montmorillonite, Chin. Sci. Bull. 55 (2010) 1092–1099.
[38] Y. Xu, W. Zhang, Subcolloidal Fe/Ag particles for reductive dehalogenation of chlorinated benzenes, Ind. Eng. Chem. Res. 39 (2000) 2238–2244.
[39] D. Mohan, K.P. Singh, S. Sinha, D. Ghosh, Removal of pyridine derivatives from aqueous solution by activated carbons developed from agricultural waste materials, Carbon 43 (2005) 1680–1693.
[40] K. Yetilmezsoy, S. Demirel, R.J. Vanderbei, Response surface modeling of Pb(II) removal from aqueous solution by *Pistacia vera* L.: Box–Behnken experimental design, J. Hazard. Mater. 171 (2009) 551–562.
[41] K.P. Singh, N. Basant, A. Malik, G. Jain, Modeling the performance of "up-flow anaerobic sludge blanket" reactor based wastewater treatment plant using linear and nonlinear approaches – a case study, Anal. Chim. Acta 658 (2010) 1–11.
[42] X. Wang, C. Chen, Y. Chang, H. Liu, Dechlorination of chlorinated methanes by Pd/Fe bimetallic nanoparticles, J. Hazard. Mater. 161 (2009)815–823.
[43] H.-L. Liu, Y.-W. Lan, Y.-C. Cheng, Optimal production of sulphuric acid by *Thiobacillus thiooxidans* using response surface methodology, Process Biochem. 39 (2004) 1953–1961.
[44] Yetilmezsoy, Kaan, Saral, Arslan, Stochastic modeling approaches based on neural network and linearnonlinear regression techniques for the determination of single droplet collection efficiency of countercurrent spray towers, Environ. Model. Assess. 12 (2007) 13–26.
[45] V. Caqueret, S. Bostyn, C. Porte, H. Fauduet, Optimization of the operating conditions for the removal of alcoholic insoluble compounds contained in sugar beet vinasse, Chem. Eng. J. 145 (2008) 203–210.
[46] D. Wu, J. Zhou, Y. Li, Effect of the sulfidation process on the mechanical properties of a $CoMoP/Al_2O_3$ hydrotreating catalyst, Chem. Eng. Sci. 64 (2009) 198–206.
[47] M.J. Hamilton, Mann-Whitney F U 2 Sample Test (a. k. a. Wilcoxon Rank Sum Test), Department of Anthropology, University of New Mexico, Albuqueque, NM, USA, 2004, September.
[48] M.J. Hamilton, 2 Sample *t*-test (1 tailed equal variance), Department of Anthropology, University of New Mexico, Albuqueque, NM, USA, 2004, September.
[49] K. Adinarayana, P. Ellaiah, Response surface optimization of the critical medium components for the production of alkaline protease by a newly isolated Bacillus sp., J. Pharmaceut. Sci. 5 (2002) 272–278.
[50] Y. Onal, C. Akmil-Basar, D. Eren, C. Sarici-Ozdemir, T. Depci, Adsorption kinetics of malachite green onto activated carbon prepared from Tunçbilek lignite, J. Hazard. Mater. 128 (2006) 150–157.
[51] K. Parkodi, K.V. Kumar, Equilibrium, kinetics and mechanism and simulation of basic and acid dyes sorption onto jute fibre carbon: eosin yellow, malechite green and crystal violet single components systems, J Hazard. Mater. 143 (2007) 311–327.
[52] B.K. Nandi, A. Goswami, M.K. Purkait, Removal of cationic dyes from aqueous solutions by kaolin: kinetic and equilibrium studies, Appl. Clay Sci. 42 (2009) 583–590.